S03120100-TRT10006
ORNL/LTR-2023/1

Oak Ridge National Laboratory Second Target Station Target Segment PIE Dose Estimates

Tucker McClanahan, Ph.D.

April 2023

Approved for public release.
Distribution is unlimited.

OAK RIDGE National Laboratory

ORNL IS MANAGED BY UT-BATTELLE LLC FOR THE US DEPARTMENT OF ENERGY

S03120100-TRT10006
ORNL/LTR-2023/1

Second Target Station Project

Second Target Station Target Segment PIE Dose Estimates

Tucker McClanahan, Ph.D.

April 2023

Prepared by
OAK RIDGE NATIONAL LABORATORY
Oak Ridge, TN 37831
managed by
UT-Battelle LLC
for the
US DEPARTMENT OF ENERGY
under contract DE-AC05-00OR22725

Second Target Station Target Segment PIE Dose Estimates

LABORATORY ORNL	DIVISION/GROUP Second Target Station (STS) Project	CALC NO. S03120100-TRT10006
Prepared by Tucker McClana-han	Level III Manager Igor Remec	Lead Engineer Steve Schrick
Other WBS elements affected		

Signature/Date

	REV 0	REV 1	REV 2	REV 3
Prepared By	Tucker McClanahan Digitally signed by Tucker McClanahan Date: 2023.05.15 09:05:27 -04'00'			
Task Leader	Tucker McClanahan Digitally signed by Tucker McClanahan Date: 2023.05.15 09:05:48 -04'00'			
Level III Manager	Igor Remec Digitally signed by 7ab68d44-0304-4215-a279-34aac517ccec Date: 2023.05.15 13:19:00 -04'00'			
Checked By	Igor Remec Digitally signed by 7ab68d44-0304-4215-a279-34aac517ccec Date: 2023.05.15 13:18:36 -04'00'			
Lead Engineer	Steven M Schrick Digitally signed by Steven M Schrick Date: 2023.05.15 09:11:04 -04'00'			

1 SCOPE

The purpose of the analysis described in this document is to support post irradiation examination (PIE) future decisions as related to the Second Target Station (STS) Project. The STS Project is discussing plans for future PIE studies, and the radionuclide inventories and dose rates included in this study will aid decision makers as they consider the need for various PIE-related machinery. Three configurations of the lasagna-type target segment are evaluated for this analysis: a single bare tungsten plate, a slice of the segment containing a single tungsten plate, and the upstream half of a segment. The lasagna type target segment used in this analysis has a precipitation hardenable nickel alloy (UNS N07718 or inconel 718) shroud, copper (C10100) cladding, and pure tungsten plates [1, 2]. The target segment is evaluated for 10 years of operation followed by two decay periods: 6 months and 2 years. For each decay period, decay gamma dose rates are tallied 30 cm from the upstream, downstream, top, bottom, and sides of the configurations. Radionuclide inventories are also provided in this report separated by material. The highest dose rates calculated in this study are 2872 rem/hr 30 cm away from the top and bottom of the half-target configuration after 6 months of decay.

2 ASSUMPTIONS AND LIMITATIONS

Initial neutron fluxes and spallation products production/destruction rates are tallied over entire parts and have not been further spatially refined. The transmutation method used in this analysis assumes that all target segments are equally irradiated during the 10 years of operation, and a more detailed discussion of the transmutation is included in Section 3.4. A single year of operation consists of four periods of 1250 hours of beam-on followed by 940 hours of beam off.

The most radioactive tungsten plate and its corresponding cladding and shroud materials are selected for the single bare tungsten plate and single slice configurations. The shroud is not subdivided in the initial particle transport calculation where the neutron fluxes and spallation products production/destruction rates are tallied. The volume-averaged decay gamma source is used for the subsection of the shroud in the half-target configuration. The volume-averaged decay gamma source for the inconel components is increased by a factor of two In order to compensate for the use of the hottest slice of the shroud surrounding the hottest tungsten plate. This factor of two was estimated based on the ratio of the gamma source strength in the hottest tungsten plate to the volume-averaged gamma source strength of all tungsten plates.

3 METHODOLOGY AND MODELS

The methodology used in this study adopts the *Position-Averaged Method* for the calculation of the rotating target activation [3]. The Monte Carlo N-Particle (MCNP) version 6.2 (MCNP6) is used to transport the proton beam, detailed in Section 3.1, through the geometry, detailed in Section 3.2, and tally the neutron fluxes and spallation products production/destruction rates using volume-averaged flux tallies and the RNUCS patch [4, 5]. These neutron fluxes and spallation products along with the material definitions discussed in Section 3.3 are then used in the transmutation calculations as discussed in Section 3.4 using CINDER2008 [6]. The resulting decay gamma sources are then transported with MCNP6 through the various geometries to calculate dose 30 cm from the surface of the various configurations as discussed in Section 3.5.

3.1 SOURCE

The high-fidelity proton source used in the initial neutron flux and spallation product calculation starts 3.0 m upstream of the outermost surface of the target, and the spatial distribution is constructed by sampling the original proton beam profile as created for the octopole magnet configuration by the accelerator systems analysis and converted to a MCNP source by Wouter de Wet. The spatial profile of the source is shown in Figure 1 and 95% of the beam falls within an area of 62.5 cm^2 on the face of the target. The proton energy is 1.3 GeV, the proton beam power is 0.7 MW, and arrives on target in pulses at a 15 Hz repetition rate resulting in a source strength of 3.3611×10^{15} protons per second.

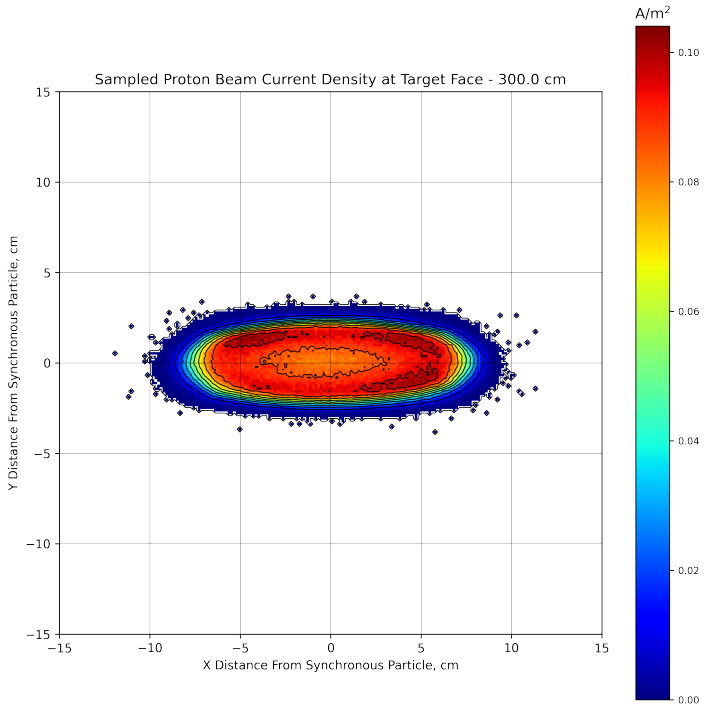

Figure 1. Proton source spatial distribution courtesy of Wouter de Wet.

This source has no angular dependence and begins each proton history parallel to the beam axis. This approximation is expected to have minimal impact on the radionuclide inventories. The source normalization factor used in this analysis is 3.3611×10^{15} protons per second. While not used in the analysis, Equation 1 shows the fitted super-Gaussian distribution for the high-fidelity spatial distribution where $\sigma_y = 1.98$ cm, $\sigma_z = 6.78$ cm, $y_0 = 0.0$ cm and $z_0 = 0.0$ cm..

$$p(y,z) = e^{-0.5\left(\frac{|y-y_0|}{\sigma_y}\right)^{6.90}} \times e^{-0.5\left(\frac{|z-z_0|}{\sigma_z}\right)^{8.09}} \quad (1)$$

3.2 GEOMETRY

Two geometries are used in support of the analysis described in this report. Section 3.2.1 discusses the geometry used in the proton beam transport where the neutron fluxes and spallation products production/destruction rates are tallied. The geometry used to calculate the decay dose rates is shown in Section 3.2.2.

3.2.1 Proton Transport Geometry

The geometry used in the initial transport of the proton source uses the full STS facility model from the target radially out to the outside of the bunker. Figure 2 shows a section view of the geometry used in the initial proton source transport. The beam direction along with the material designations have been noted.

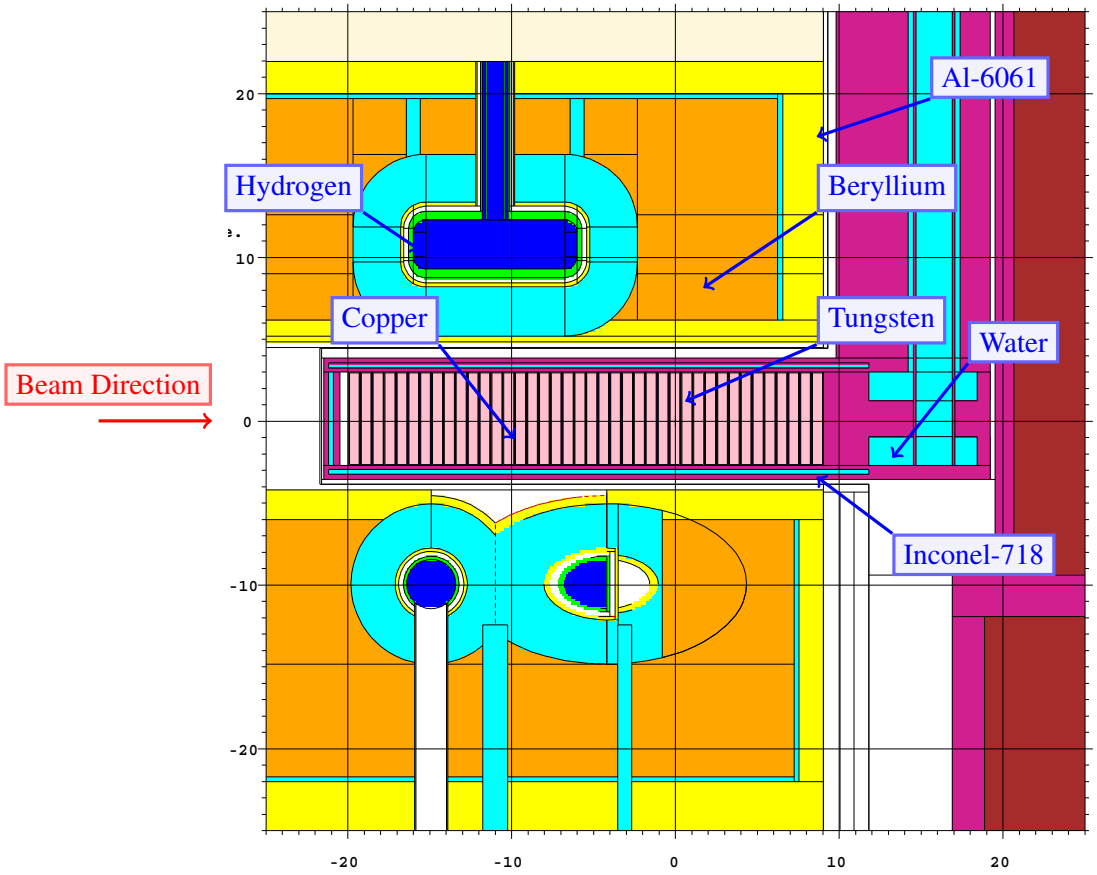

Figure 2. Cross section view of the MCNP6 geometry used in the initial proton source transport where the proton beam direction and material designations have been marked.

3.2.2 Decay Dose Geometry

Three configurations are evaluated in support of STS target PIE considerations: a single tungsten slab, single target slice, and the upstream half of the target segment. Decay dose for each configuration is calculated for 6 months and 2 years of decay after last beam-on-target following 10 years of operation. All geometry figures for the decay dose calculations are included in Appendix A.

Figures A.1 & A.2 show the single tungsten slab geometry used in the decay dose calculations. The most radioactive (highest decay gamma source strength) slab is selected for this analysis and is the sixth tungsten slab along the beam direction (See Figure 2). Overall dimensions of the bare tungsten slab are 5.6×14×0.6 cm (H×W×D).

Figures A.3, A.4, & A.5 show the single slice geometry that has the most radioactive tungsten plate surrounded by copper cladding and inconel-718 shroud. Each figure has the materials and orientation noted on the figure. The water in the water cooling channels has been drained for the decay dose calculations. Figure A.3 shows the water channels cut through the inconel-718 shroud above and below the tungsten slab. Figure A.4 shows a plan view of the single slice geometry with the beam direction noted. Figure A.5 shows a side section view of the single slice geometry with the copper cladding clearly surrounding the tungsten plate. Overall dimensions of the slice are 7.4×16×0.7 cm (H×W×D).

Figures A.6, A.7, & A.8 show the upstream half of the lasagna target segment consisting of 20 copper clad tungsten slabs all surrounded by a water-cooled inconel-718 shroud. Materials, beam direction, and orientation indicators have been included for each figure. Figure A.6 shows a cross section view of the half segment geometry showing the empty water cooling channels above and below the tungsten slabs. Figure A.7 shows all 20 tungsten slabs and the upstream empty water channel. Figure A.8 shows the 20 tungsten slabs along beam center.

3.3 MATERIALS

The materials used in support of the study are included in Appendix B. ENDF/B-VII.1 continuous energy cross sections are used in the initial proton beam transport and the decay dose MCNP6 calculations, and the 321 energy group flat-weighted CINDER2008 cross section library is used during the transmutation [7].

3.4 TRANSMUTATION

This section outlines the details of the transmutation mechanics used to compute the radionuclide inventories and decay gamma spectra for each configuration. Figure 3 shows the rigorous two-step (R2S) method used to calculate the radionuclide inventories. The R2S method begins by utilizing MCNP6 to transport the proton source and tally the neutron fluxes and spallation products in the regions of interest. These neutron fluxes and spallation products are fed into CINDER2008 to produce radionuclide inventories and decay gamma sources for two decay time steps following 10 years of operation: 6 months and 2 years. One operating year is assumed to consist of four sets of beam on and beam off, where a set is 1250 hr beam on and 940 hr beam off.

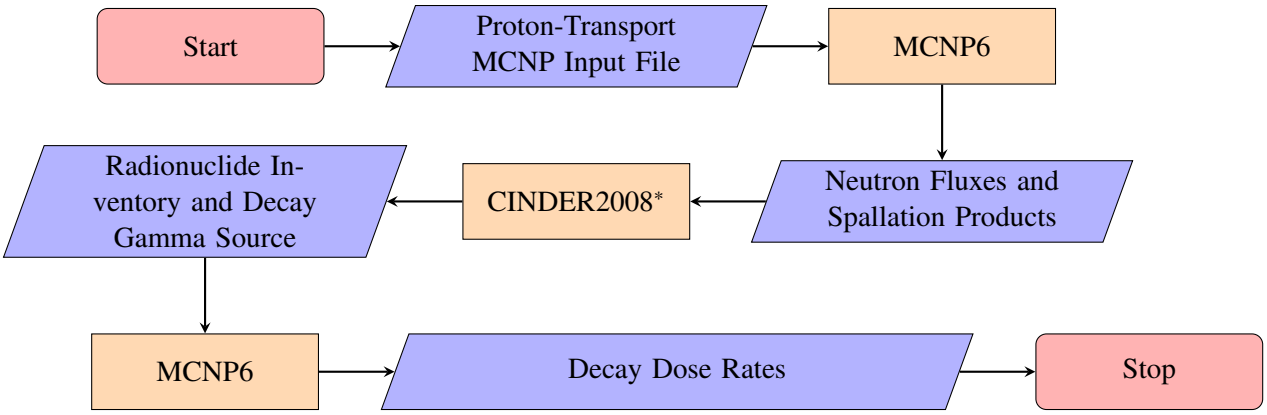

Figure 3. R2S Transmutation Workflow where the CINDER2008* refers to using the "Position-Averaged" method described in ORNL/TM-2022/2639 [3]

The neutron fluxes are tallied in the CINDER90's 63 energy-group structure which differs from the 321 energy-group structure CINDER2008 uses in the flat-weighted cross section set. The 63 energy-group binning of the neutron fluxes is chosen to be consistent with previous STS analysis, and to have better convergence when compared to tallying with 321 energy groups. With the analysis described in this report being preliminary in nature, the coarse energy binning was deemed acceptable since a brief study showed that by using the same 63-group energy binning structure as CINDER90, the activation quantities are more consistent with previous STS analysis. However, more detailed and final transmutation analysis will bin the neutron fluxes with the 321-group energy structure. Another brief study showed that activation quantities were higher (conservative) by factors of 1.5-2 if fluxes were binned in 63 energy groups compared to the case using 321 energy groups, when CINDER2008 321-group flat-weighted cross sections are used in both cases. The neutron fluxes binned with 321 energy groups were closer to the MCNP6-calculated quantity in the brief study. By binning with 321 energy groups, the resonance-effects of the cross sections are better captured, and result in more accurate activation quantities.

The "Position-Averaged" method described in ORNL/TM-2022/2639 is used to calculate the radionuclide inventory in a single target segment [3]. The target shroud is not subdivided into the configurations until after the initial proton transport calculation is completed. In order to implement the three configurations, the volume used for the inconel-718 shroud transmutation is altered to reflect the volume corresponding to the specific configuration. The volume-averaged fluxes and spallation product production and destruction rates are then scaled by this updated volume of the shroud. This assumption is discussed in Section 2.

The resulting radionuclide inventories are processed using a python script that utilizes the utilities included in the ACTIUM Python Toolkit [8]. The python script produces Excel spreadsheets for every configuration for every material. These spreadsheets are discussed in Section 4. The decay gamma emissions are used as the source in the decay gamma dose rate calculations discussed in Section 3.5.

3.5 DECAY DOSE CALCULATIONS

Decay dose rates were calculated by transporting the decay gamma sources calculated by the activation workflow described in Section 3.4 using MCNP6 to six locations around each configuration. The geometry used in the decay dose calculations is discussed in Section 3.2.2. The six locations are 30 cm above, below,

to the side(s), upstream, and downstream of the exterior surface of the configurations. All locations are centered to the configuration. At each location, a point detector next event estimator is positioned to tally the photon flux at that point. The photon flux is then folded with the response function shown in Table C.1 in Appendix C using the *de* and *df* cards in MCNP6 to allow output of the dose rates directly from MCNP6.

4 ANALYSIS AND RESULTS

Each of the following sections identifies which *.zip.txt* file corresponds with the results for a single configuration. The *.zip.txt* files electronically attached to this document are accessible by using a PDF viewer that supports PDF attachment such as Adobe Acrobat, Adobe Reader, Firefox etc. Each spreadsheet in the *.zip.txt* files contains radionuclide inventories for each decay period. Once the reader downloads the *.zip.txt* files, the reader must delete the *.txt* from the filename before opening the *.zip* files.

All dose rates reported in this section are the calculated dose rates plus two sigma from the statistical error in the MCNP6 transport. The relative errors for all dose rates are below 1%.

4.1 SINGLE TUNGSTEN SLAB RESULTS

The attached *Single_Tungsten_Slab_Spreadsheets.zip.txt* contains the full radionuclide inventory activity data separated by material in spreadsheets along with a spreadsheet containing the dose rates for the single tungsten slab configuration. Table 1 shows an overview of the single tungsten slab transmutation data for the two decay periods.

Table 1. Single Tungsten Slab Activity Overview

Material	**Mass (g)**	**Decay 6 Months Activity (Ci)**	**Decay 2 Years Activity (Ci)**
Tungsten	9.03E+02	1.26E+02	4.79E+01
Total Mass (g)	9.03E+02		
Total Activity (Ci)		1.26E+02	4.79E+01
Total Decay Power (W)		1.15E-01	3.76E-02

Table 2 shows the dose rates for the single tungsten slab configuration for each of the locations discussed above. Tallies above and below the slab resulted in the same dose rate due to the symmetry of the geometry. The same can be said for the tallies that are to the sides of the configuration. The dose rates in the single tungsten slab configuration are driven by spallation products in the tungsten. The highest dose rates for the single tungsten slab configuration are observed 30 cm from the upstream and downstream face of the configuration.

Table 2. Dose Estimates 30 cm from Surface for Single Tungsten Slab

Location	6 Months Decay Dose (mrem/hr)	2 Year Decay Dose (mrem/hr)
Above/Below	7.9956E+03	3.4265E+03
Downstream	3.9333E+04	1.6672E+04
Upstream	3.9985E+04	1.6939E+04
Side	3.3775E+03	1.4424E+03

*Dose rates reported are mean plus two sigma

4.2 SINGLE TARGET SLICE RESULTS

The attached *Single_Slice_Spreadsheets.zip.txt* contains the full radionuclide inventory activity data separated by material in spreadsheets along with a spreadsheet containing the dose rates for the single target slice configuration. Table 3 shows an overview of the single target slice transmutation data for the two decay periods.

Table 3. Single Slice Activity Overview

Material	Mass (g)	Decay 6 Months Activity (Ci)	Decay 2 Years Activity (Ci)
Tungsten	9.03E+02	1.26E+02	4.79E+01
Copper	8.17E+01	5.15E+00	3.68E+00
Inconel-718	1.29E+02	3.85E+01	1.11E+01
Total Mass (g)	1.11E+03		
Total Activity (Ci)		1.70E+02	6.27E+01
Total Decay Power (W)		4.63E-01	1.57E-01

Table 4 shows the dose rates for the single target slice configuration for each of the locations discussed above. Tallies above and below the slab resulted in the same dose rate due to the symmetry of the geometry. The same can be said for the tallies that are to the sides of the configuration. The dose rates are much higher than the single tungsten slab configuration largely due to the presence of the inconel-718 and the radioactive nickel and cobalt isotopes within. The highest dose rates for the single target slice configuration are observed either 30 cm upstream and downstream of the configuration.

Table 4. Dose Estimates 30 cm from Surface for Single Slice

Location	6 Months Decay Dose (mrem/hr)	2 Year Decay Dose (mrem/hr)
Above/Below	2.3069E+05	8.5294E+04
Downstream	5.1253E+05	1.9216E+05
Upstream	5.1380E+05	1.9012E+05
Side	1.2127E+05	4.4102E+04

*Dose rates reported are mean plus two sigma

4.3 HALF TARGET SEGMENT RESULTS

The attached *Half_Target_Segment_Spreadsheets.zip.txt* contains the full radionuclide inventory activity data separated by material in spreadsheets along with a spreadsheet containing the dose rates for the upstream half of the target segment configuration. Table 5 shows an overview of the upstream half of the target segment transmutation data for the two decay periods.

Table 5. Half Target Segment Activity Overview

Material	Mass (g)	Decay 6 Months Activity (Ci)	Decay 2 Years Activity (Ci)
Tungsten	1.68E+04	2.06E+03	7.50E+02
Copper	1.52E+03	8.25E+01	5.84E+01
Inconel-718	3.30E+03	9.08E+02	2.68E+02
Total Mass (g)	2.16E+04		
Total Activity (Ci)		3.05E+03	1.08E+03
Total Decay Power (W)		9.82E+00	3.27E+00

Table 6 shows the dose rates for the upstream half of the target segment configuration for each of the locations discussed above. Tallies above and below the slab resulted in the same dose rate due to the symmetry of the geometry. The same can be said for the tallies that are to the sides of the configuration. This configuration has the highest dose rates when compared to the other two configurations due to the increased amount of inconel-718 in the configuration. The upstream dose rate is approximately twice as high as the downstream dose rate due to the lack of inconel-718 on the downstream end of the configuration. The highest dose rates for the upstream half of the target segment are observed 30 cm above and below of exterior of the target segment.

Table 6. Dose Estimates 30 cm from Surface for Half Target Segment

Location	6 Months Decay Dose (mrem/hr)	2 Year Decay Dose (mrem/hr)
Above/Below	2.8721E+06	1.0560E+06
Downstream	9.8247E+05	3.7988E+05
Upstream	1.8956E+06	6.8128E+05
Side	1.3616E+06	5.1048E+05

*Dose rates reported are mean plus two sigma

5 CONCLUSIONS

The transmutation of the STS lasagna target concept has been evaluated for 10 years of operation followed two decay periods: 6 months and 2 years. Dose rates and radionuclide inventories for each decay period have been calculated in support of STS PIE decision makers. Three PIE configurations of the lasagna target were considered in this report: a single bare tungsten plate, a slice of the segment containing a single tungsten plate, and the upstream half of the target segment. The highest dose rates were observed 30 cm above and below the upstream half of the target segment configuration. The high dose rates are largely attributed to the activated inconel-718 shroud. The lowest dose rates and overall activation levels were observed with the single bare tungsten plate configuration.

References

[1] "Standard Specification for Precipitation-Hardening Nickel Alloy (UNS N07718) Plate, Sheet, and Strip for High-Temperature Service," Nov. 2007. ASTM B670-07.

[2] "Standard Specification for Copper Sheet, Strip, Plate, and Rolled Bar," 2019. ASTM B152/B152M-19.

[3] T. McClanahan and I. Remec, "Second Target Station High-Fidelity Target Activation Comparison," Tech. Rep. ORNL/TM-2022/2639, 2022.

[4] C. J. Werner, J. Armstrong, S. G. Mashnik, G. W. McKinney, F. B. Brown, M. E. Rising, G. E. McMath, J. S. Bull, C. Solomon, J. S. Hendricks, L. Casswell, A. Sood, D. B. Pelowitz, L. J. Cox, J. E. Sweezy, R. E. Prael, D. Dixon, C. J. Werner, T. E. Booth, R. A. Forester, A. Zukaitis, M. R. James, J. T. Goorley, C. Anderson, M. L. Fensin, H. G. Hughes, J. S. Elson, T. A. Wilcox, J. Favorite, J. W. Durkee, B. C. Kiedrowski, R. Martz, and R. C. Johns, "MCNP User's Manual Code Version 6.2," Tech. Rep. LA-UR-17-29981, Oct. 2017.

[5] B. J. Micklich, "CINDER2008 – A New Version of CINDER," in *3rd International Workshop on Accelerator Radiation Induced Activation*, (Knoxville, TN), ARIA, 2015.

[6] S. Holloway, W. Wilson, C. Kelsey, H. Little, V. Mozin, and T. England, "A Manual for CINDER2008 Codes and Data," Tech. Rep. LA-UR-11-00006, Jan. 2011.

[7] M. Chadwick and et. al, "ENDF/B-VII.1 Nuclear Data for Science and Technology: Cross Sections, Covariances, Fission Product Yields and Decay Data," *Nuclear Data Sheets*, vol. 112, no. 12, pp. 2887 – 2996, 2011. Special Issue on ENDF/B-VII.1 Library.

[8] T. McClanahan, T. Goorley, and J. Auxier II, "Hiroshima and Nagasaki Verification of an Unstructured Mesh based Transmutation Toolkit," *Nuclear Technology*, pp. 1–18, 2020.

[9] I. Popova, "Flux to Dose Conversion Factors," Tech. Rep. SNS-NFDD-NSD-TR-0001, R00, Mar. 2010.

APPENDIX A. DECAY DOSE GEOMETRY FIGURES

APPENDIX A. DECAY DOSE GEOMETRY FIGURES

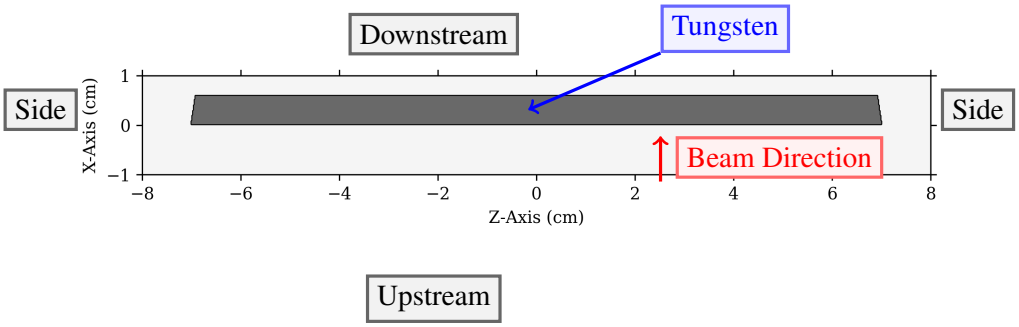

Figure A.1. Plan view of the single tungsten slab geometry through middle of slab

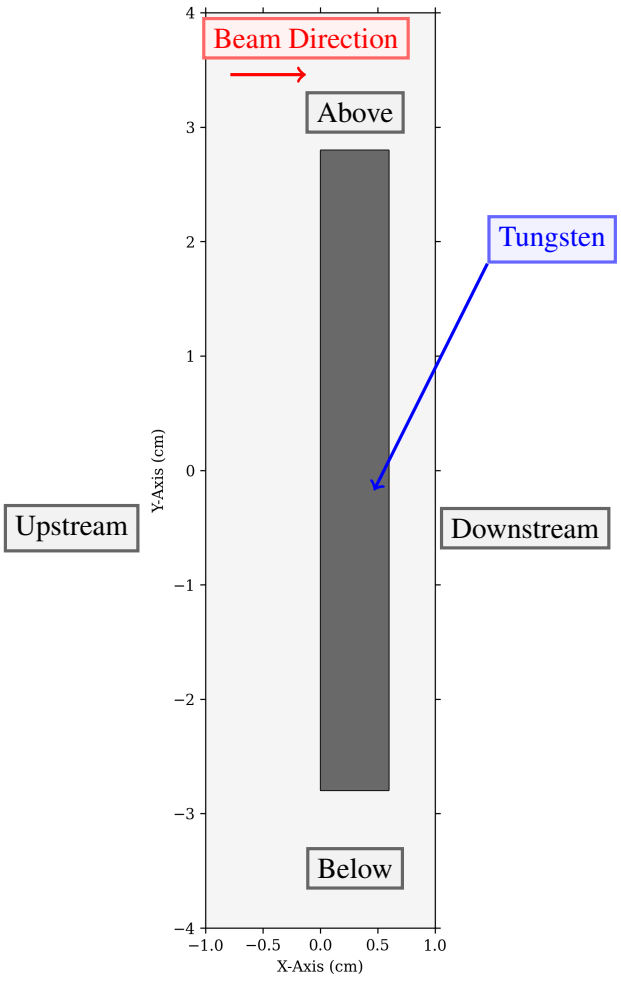

Figure A.2. Side section view of the single tungsten slab geometry

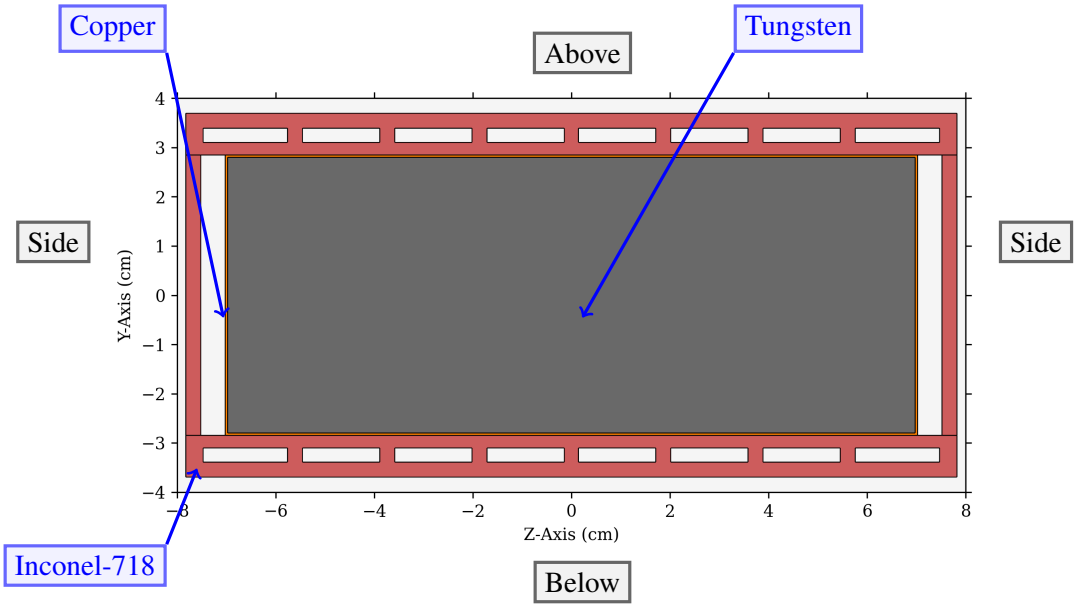

Figure A.3. Cross section view of the single slice geometry through middle of slice

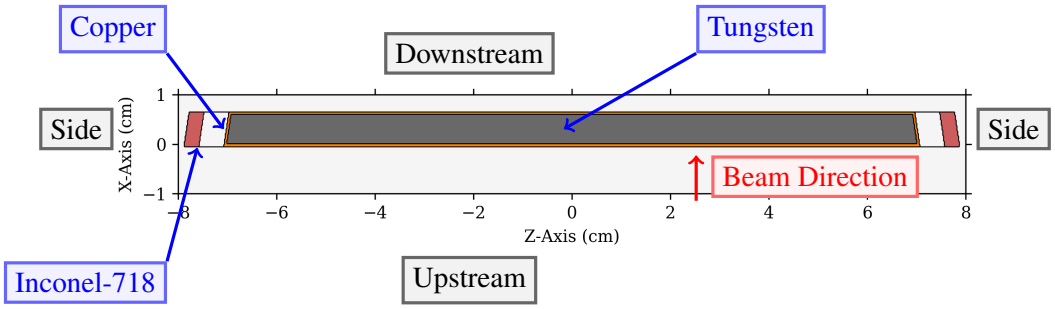

Figure A.4. Plan view of the single slice geometry through middle of slice

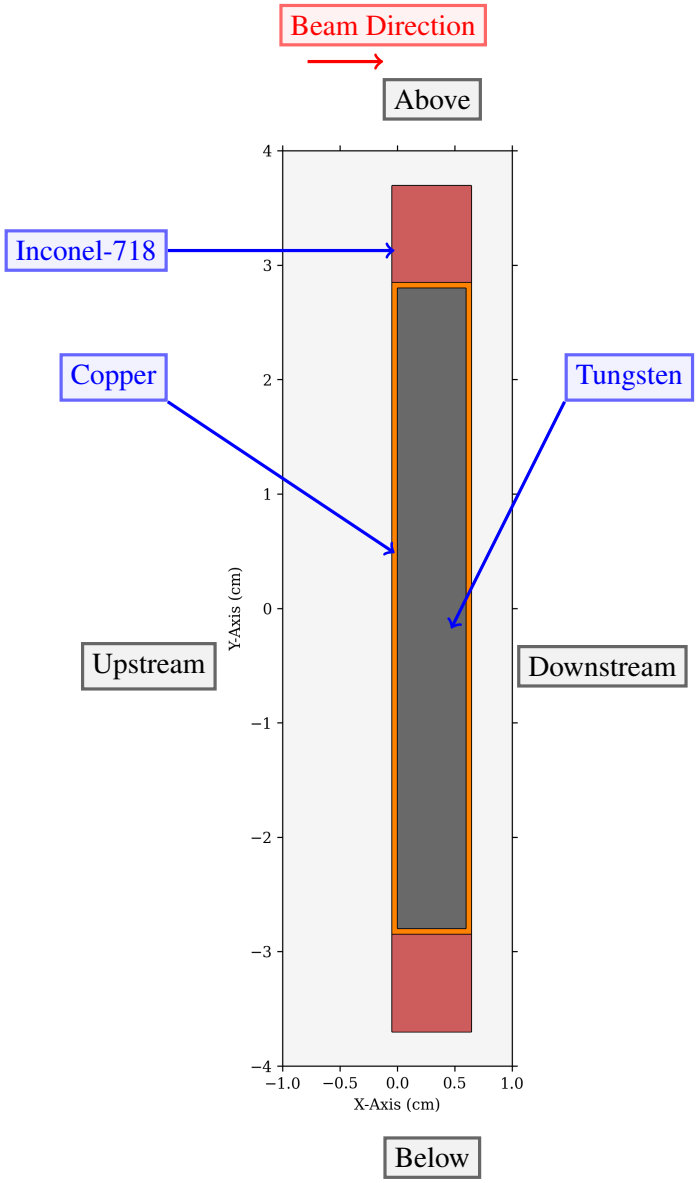

Figure A.5. Side section view of the single slice geometry through middle of slice

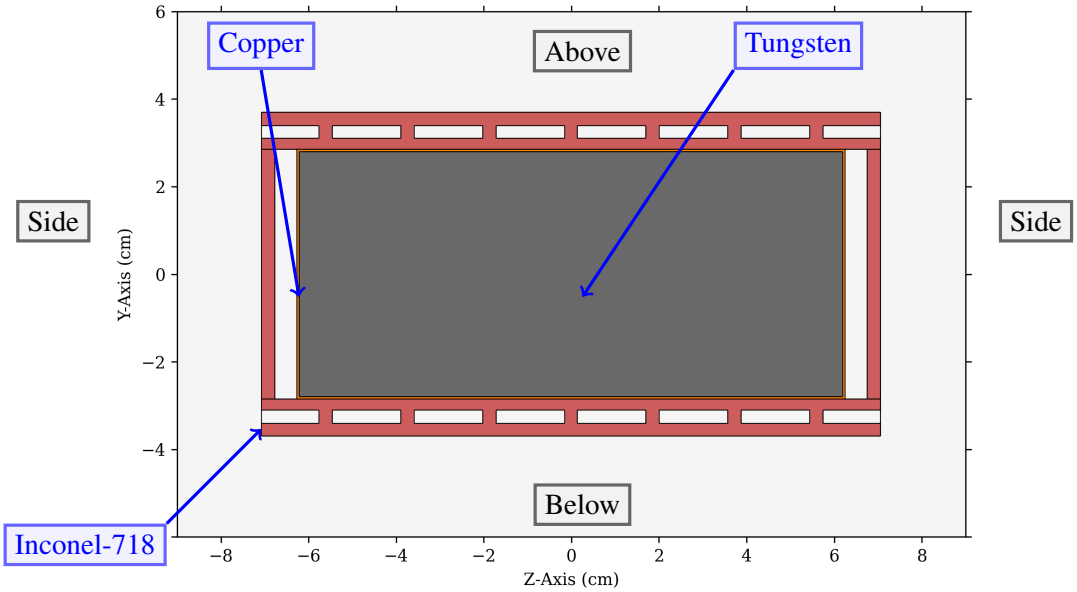

Figure A.6. Cross section view of the half segment geometry

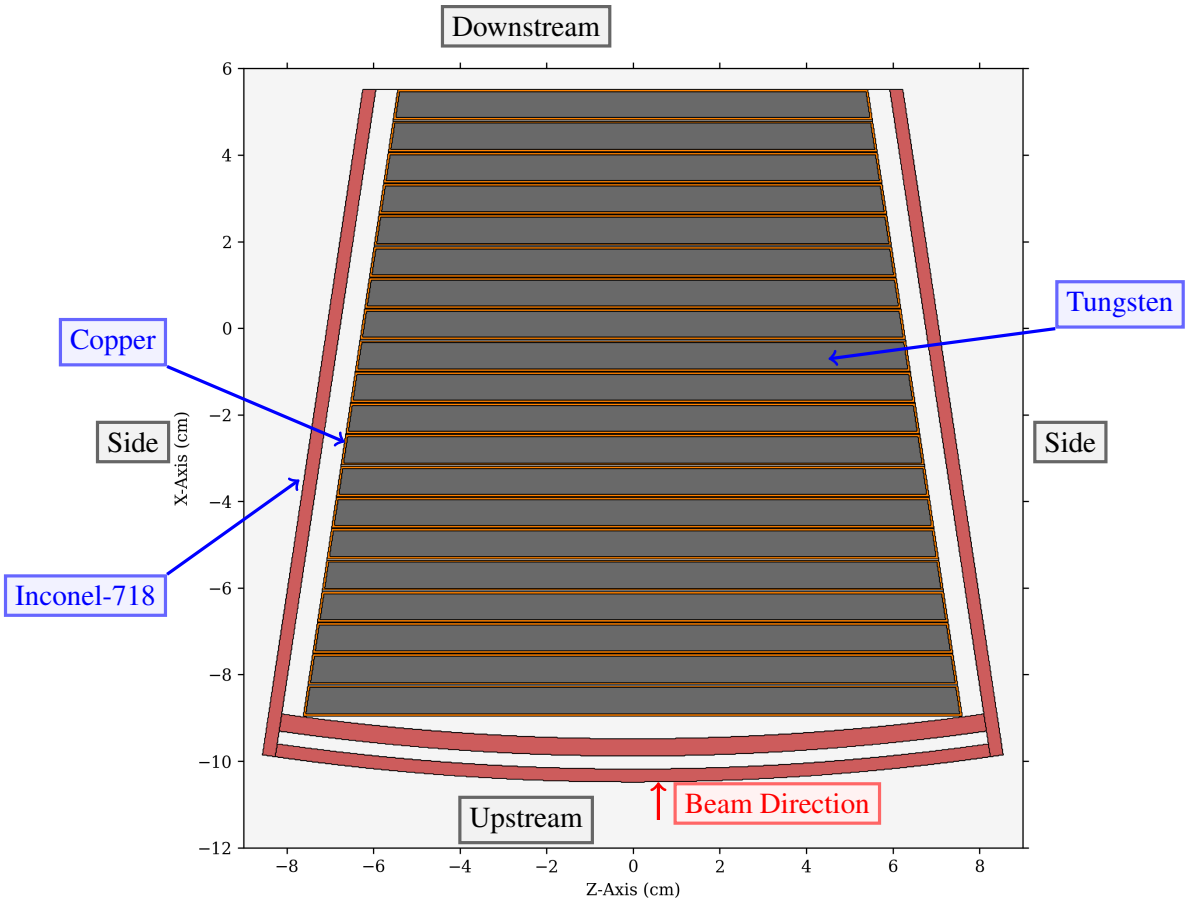

Figure A.7. Plan view of the half segment geometry

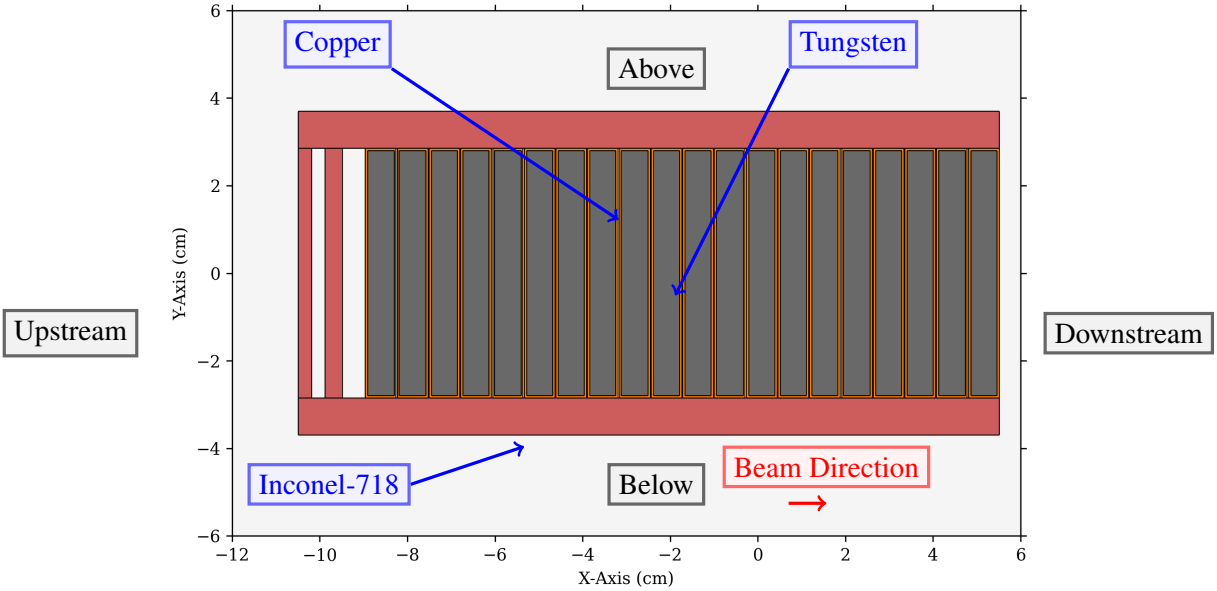

Figure A.8. Side section view of the half segment geometry

APPENDIX B. MATERIAL DEFINITION

APPENDIX B. MATERIAL DEFINITION

Table B.1. Tungsten Material Definition

Nuclide	Mass Fraction	Atom Fraction
^{180}W	1.1451E-03	1.1700E-03
^{182}W	2.5955E-01	2.6227E-01
^{183}W	1.4171E-01	1.4241E-01
^{184}W	3.0674E-01	3.0658E-01
^{186}W	2.9085E-01	2.8757E-01
Density (g/cm^3)	19.3	

Table B.2. Copper Material Definition

Nuclide	Mass Fraction	Atom Fraction
^{16}O	4.989538E-06	1.982246E-05
^{17}O	2.019813E-09	7.550290E-09
^{18}O	1.149894E-08	4.059613E-08
^{31}P	2.999723E-06	6.154125E-06
^{32}S	1.419869E-05	2.821997E-05
^{33}S	1.159893E-07	2.235419E-07
^{34}S	6.749376E-07	1.262625E-06
^{36}S	1.679845E-09	2.967858E-09
^{55}Mn	4.999538E-07	5.782769E-07
^{54}Fe	5.649477E-07	6.655484E-07
^{56}Fe	9.189150E-06	1.043930E-05
^{57}Fe	2.159800E-07	2.410518E-07
^{58}Fe	2.929729E-08	3.213502E-08
^{58}Ni	6.719378E-06	7.369953E-06
^{60}Ni	2.679752E-06	2.841344E-06
^{61}Ni	1.179891E-07	1.230502E-07
^{62}Ni	3.829646E-07	3.929600E-07
^{64}Ni	1.009907E-07	1.003852E-07
^{63}Cu	6.849366E-01	6.916313E-01
^{65}Cu	3.149709E-01	3.082613E-01
^{64}Zn	4.719564E-07	4.691181E-07
^{66}Zn	2.819739E-07	2.717886E-07
^{67}Zn	4.199612E-08	3.987366E-08
^{68}Zn	1.979817E-07	1.852147E-07
^{70}Zn	6.749376E-09	6.133500E-09
^{75}As	4.999537E-06	4.240353E-06
^{74}Se	2.499769E-08	2.148832E-08
^{76}Se	2.699750E-07	2.259701E-07
^{77}Se	2.229794E-07	1.842066E-07
^{78}Se	7.039349E-07	5.740870E-07
^{80}Se	1.509860E-06	1.200548E-06

Table B.2 – continued from previous page

Nuclide	Mass Fraction	Atom Fraction
^{82}Se	2.719748E-07	2.109772E-07
^{107}Ag	1.279882E-05	7.607651E-06
^{109}Ag	1.219887E-05	7.117902E-06
^{106}Cd	1.179891E-08	7.079435E-09
^{108}Cd	8.539210E-09	5.028733E-09
^{110}Cd	1.219887E-07	7.053251E-08
^{111}Cd	1.259883E-07	7.218745E-08
^{112}Cd	2.399778E-07	1.362729E-07
^{113}Cd	1.229886E-07	6.922027E-08
^{114}Cd	2.909731E-07	1.623288E-07
^{116}Cd	7.719286E-08	4.232092E-08
^{112}Sn	1.829831E-08	1.039062E-08
^{114}Sn	1.269883E-08	7.084487E-09
^{115}Sn	6.579392E-09	3.638583E-09
^{116}Sn	2.839737E-07	1.556924E-07
^{117}Sn	1.509860E-07	8.207114E-08
^{118}Sn	4.809555E-07	2.592175E-07
^{119}Sn	1.719841E-07	9.191228E-08
^{120}Sn	6.579391E-07	3.486886E-07
^{122}Sn	9.509120E-08	4.956825E-08
^{124}Sn	1.209888E-07	6.204897E-08
^{121}Sb	2.269790E-06	1.192957E-06
^{123}Sb	1.729840E-06	8.943723E-07
^{120}Te	1.689844E-09	8.955544E-10
^{122}Te	4.869549E-08	2.538361E-08
^{123}Te	1.709842E-08	8.840323E-09
^{124}Te	9.209148E-08	4.722995E-08
^{125}Te	1.379872E-07	7.020051E-08
^{126}Te	3.719656E-07	1.877348E-07
^{128}Te	6.359412E-07	3.159442E-07
^{130}Te	6.939358E-07	3.394443E-07
^{204}Pb	6.889363E-08	2.146276E-08
^{206}Pb	1.199889E-06	3.701748E-07
^{207}Pb	1.099898E-06	3.376851E-07
^{208}Pb	2.629757E-06	8.034894E-07
^{209}Pb	9.999075E-07	3.040419E-07
Density (g/cm^3)	8.93	

Table B.3. Inconel-718 Material Definition

Nuclide	Mass Fraction	Atom Fraction
^{10}B	1.109244E-05	6.496927E-05
^{11}B	4.906655E-05	2.613774E-04
^{12}C	7.924598E-04	3.872919E-03
^{13}C	9.283671E-06	4.187037E-05
^{27}Al	8.014536E-03	1.742024E-02
^{28}Si	3.217806E-03	6.745317E-03
^{29}Si	1.698842E-04	3.438346E-04
^{30}Si	1.159210E-04	2.268105E-04
^{31}P	1.498978E-04	2.838205E-04
^{32}S	1.419033E-04	2.602939E-04
^{33}S	1.159210E-06	2.061894E-06
^{34}S	6.765388E-06	1.168065E-05
^{36}S	1.688849E-08	2.753772E-08
^{46}Ti	9.123780E-04	1.164413E-03
^{47}Ti	8.404271E-04	1.049761E-03
^{48}Ti	8.504203E-03	1.040174E-02
^{49}Ti	6.375654E-04	7.638945E-04
^{50}Ti	6.225756E-04	7.310454E-04
^{50}Cr	7.105156E-03	8.342860E-03
^{52}Cr	1.429026E-01	1.613527E-01
^{53}Cr	1.648876E-02	1.826590E-02
^{54}Cr	4.177153E-03	4.541725E-03
^{55}Mn	3.507609E-03	3.744384E-03
^{54}Fe	8.564161E-03	9.311496E-03
^{56}Fe	1.389053E-01	1.456391E-01
^{57}Fe	3.277766E-03	3.376276E-03
^{58}Fe	4.436975E-04	4.491603E-04
^{59}Co	9.993187E-03	9.944581E-03
^{58}Ni	3.707472E-01	3.752985E-01
^{60}Ni	1.478992E-01	1.447299E-01
^{61}Ni	6.515558E-03	6.271268E-03
^{62}Ni	2.108563E-02	1.996822E-02
^{64}Ni	5.556212E-03	5.097185E-03
^{63}Cu	2.058597E-03	1.918487E-03
^{65}Cu	9.473542E-04	8.557052E-04
^{92}Mo	4.676812E-03	2.984315E-03
^{94}Mo	2.987963E-03	1.866073E-03
^{95}Mo	5.196458E-03	3.211122E-03
^{96}Mo	5.516240E-03	3.373228E-03
^{97}Mo	3.187827E-03	1.929241E-03
^{98}Mo	8.164434E-03	4.890597E-03
^{100}Mo	3.327731E-03	1.953407E-03
^{181}Ta	5.256417E-02	1.703642E-02
Density (g/cm^3)	8.19	

APPENDIX C. FLUX-TO-DOSE CONVERSION FACTORS

APPENDIX C. FLUX-TO-DOSE CONVERSION FACTORS

Table C.1. Extended ICRP-74 Photon Flux-To-Dose Conversion Factors for Effective Dose [9]

Energy (MeV)	**Factor** ($\frac{mrem/hr}{\gamma/cm^2/sec}$)
1.0000E-02	1.7466E-05
1.5000E-02	4.5153E-05
2.0000E-02	7.3786E-05
3.0000E-02	1.0798E-04
4.0000E-02	1.2170E-04
5.0000E-02	1.2861E-04
6.0000E-02	1.3608E-04
8.0000E-02	1.5838E-04
1.0000E-01	1.8618E-04
1.5000E-01	2.7084E-04
2.0000E-01	3.6147E-04
3.0000E-01	5.4300E-04
4.0000E-01	7.1850E-04
5.0000E-01	8.8764E-04
6.0000E-01	1.0469E-03
8.0000E-01	1.3417E-03
1.0000E+00	1.6140E-03
1.5000E+00	2.2104E-03
2.0000E+00	2.6963E-03
3.0000E+00	3.5587E-03
4.0000E+00	4.3255E-03
5.0000E+00	5.0405E-03
6.0000E+00	5.7554E-03
8.0000E+00	7.1709E-03
1.0000E+01	8.5536E-03
1.5000E+01	1.0080E-02
2.0000E+01	1.1880E-02
3.0000E+01	1.4760E-02
4.0000E+01	1.6920E-02
5.0000E+01	1.8720E-02
1.0000E+02	2.3760E-02
2.0000E+02	2.7720E-02
5.0000E+02	3.1680E-02
1.0000E+03	3.3480E-02
2.0000E+03	3.4560E-02
5.0000E+03	3.5640E-02
1.0000E+04	3.6360E-02

APPENDIX C. COMPUTER HARDWARE AND SOFTWARE

APPENDIX C. COMPUTER HARDWARE AND SOFTWARE

The Saturn computing cluster at STS was used to perform the analysis discussed in this report. The cinder/2008 and mcnp/mcnp6.2rnucs_20220627 modules were used to load the appropriate CINDER and MCNP6 codes and their corresponding software libraries.

APPENDIX D. LOCATION OF COMPUTATIONAL INPUT AND OUTPUT FILES

APPENDIX D. LOCATION OF COMPUTATIONAL INPUT AND OUTPUT FILES

The location of all of the files used to generate the analysis described in this report are located on the Saturn computing cluster hosted at STS in the following compressed archive file: /home/sts_archive/S.03.10_Remote_Hand/S03120100-TRT10006_Target_PIE_Dose_Rates/S03120100-TRT10006_Target_PIE_Dose_Rates.tar.gz